Geomechanics and Engineering, *Vol. 39, No. 3 (2024) 305-316*
https://doi.org/10.12989/gae.2024.39.3.305

Numerical simulation and experimental analysis of granite residual soil-concrete interface under cyclic shear

Feiyu Liu*[1,2], Kechao Ma[1a] and Wei Yu[3b]

[1]*School of Mechanics and Engineering Sciences, Shanghai University, Shanghai 200444, China*
[2]*School of Civil Engineering and Architecture, East China Jiaotong University, Nanchang 330013, China*
[3]*Zhejiang Huadong Geotechnical Investigation and Design Institute Co., Ltd., Hangzhou, Zhejiang 310030, China*

(*Received July 2, 2024, Revised October 18, 2024, Accepted Octoebr 22, 2024*)

Abstract. Pile foundations are frequently subjected to dynamic loads, necessitating a thorough investigation of cyclic shear characteristics at pile-soil interfaces. To investigate the influence of soil moisture content and concrete surface roughness on the cyclic shear characteristics of interfaces, a series of cyclic shear tests were conducted using a large-scale indoor direct shear apparatus. The effects of three normal stresses (100, 200, and 300 kPa), four moisture content levels (14%, 19%, 24%, and 29%), and five concrete surface joint roughness coefficients (0.4, 5.8, 9.5, 12.8, and 16.7) on interface shear stress and volumetric strain behavior of residual soil were analyzed. Numerical simulations were employed to analyze the microstructural changes in particles. The results show that the water content has a significant effect on the interface stress-displacement curve. It shows a cyclic hardening type at low water content and a cyclic softening type at high water content. There is a critical roughness on the concrete surface. After exceeding this value, the shear strength of the interface is no longer improved. The number of force chains in the soil increases with the increase of the number of cycles and roughness. The increase of the number of particles in the force chain leads to the increase of the instability of the force chain structure. Therefore, most of the force chains are composed of three particles. The main direction of the normal and tangential contact force anisotropy is closely related to the shear direction. The main direction will deflect with the shear direction, and the deflection angle is about 35°.

Keywords: direct shear test; moisture content; numerical simulation; roughness; soil-structure interface

1. Introduction

In engineering practice, the issue of structural failure and soil deformation due to the interaction between soil and structures is becoming increasingly prominent (Yang *et al.* 2023). For instance, in pile foundation engineering, the pile foundation is subjected to external loads such as buoyancy from groundwater, vehicles, waves, and earthquakes (Li *et al.* 2022a). These loads are primarily transmitted through the soil-structure interface (Chen *et al.* 2022). Therefore, understanding the mechanical characteristics between piles and soil is crucial for engineering design and analysis (Wang *et al.* 2021).

Domestic and international scholars have conducted in-depth research on the mechanisms and influencing factors of soil-structure interaction through various indoor experiments. Mirzaalimohammadi *et al.* (2019) explored the interaction between fine sand and geosynthetics using pull-out tests, finding that the application of GGB and GCP systems increased the geosynthetic-soil interaction force by 37% and 46%, respectively. Dou *et al.* (2023) investigated the mechanical properties of rock-soil interfaces through a series of ring shear tests, concluding that the main factors affecting interface shear strength are water content and roughness. Liu *et al.* (2021a) proposed a triaxial test method with a pre-set failure surface to create composite samples of soil and structure, discovering that the interface friction angle obtained from direct shear tests was lower than that from triaxial tests. Maghsoodi *et al.* (2020) studied the influence of temperature on the shear behavior of clay-structure interfaces through direct shear tests, revealing that increasing temperature slows the rate of strain accumulation and extends the structural cycle life by 2 to 3 times. Although direct shear tests have the disadvantage of uneven stress distribution, they remain widely used for studying soil-structure interfaces due to their practicality and convenience.

Given that pile foundation engineering is subjected to various cyclic loads, understanding the cyclic response of the soil-structure interface is of great significance. Liu *et al.* (2021b) investigated the effect of horizontal cyclic loads on the maximum shear stiffness and ultimate damping ratio of the geosynthetic-soil interface under different normal stresses. Qi *et al.* (2023) conducted comparative tests of monotonic direct shear and post-cyclic monotonic direct shear, revealing the enhancement effect of cyclic shear on interface shear strength. Ying *et al.* (2022) further analyzed the cyclic shear characteristics of the geosynthetic-soil interface under cyclic loading and unloading, indicating that

*Corresponding author, Professor
E-mail: lfyzju@shu.edu.cn
[a]Student
E-mail: mkc@shu.edu.cn
[b]Senior Engineer
E-mail: 408379275@qq.com

ISSN: 2005-307X (Print), 2092-6219 (Online)

with the increase in cyclic normal load amplitude, shear stiffness, enhancement coefficient, and relative displacement all exhibited increasing trends. Liu *et al.* (2021c) studied the influence of normal loading frequency on interface mechanical properties, demonstrating periodic dynamic changes in shear stress and normal displacement, with the shear stress amplitude decreasing as the frequency increased. Li *et al.* (2022b) investigated the effects of sinusoidal, oblique, and square wave loads on hysteresis loops under bidirectional cyclic horizontal and normal loading. Most experiments are limited to unidirectional shear paths, whereas Feng *et al.* (2022) delved into the effects of circular shear paths on tangential displacement, non-coaxial angles, and shear flexibility at the interface. Overall, compared to static shear, the study of cyclic shear characteristics at the soil-structure interface remains insufficient.

Traditional experimental methods are constrained by size and observation limitations, while the discrete element method (DEM) has the advantage of capturing microscopic contact behavior between particles, providing detailed experimental parameters to reveal the interaction mechanisms at the soil-structure interface (Chen *et al.* 2023). For static loads, scholars have used DEM to study the effects of roughness (Fang *et al.* 2020), particle crushing (Li *et al.* 2023), particle sphericity (Zhou *et al.* 2019), and soil type (Mamen and Hammoud 2021) on interface mechanical properties. Regarding cyclic loads, Liu *et al.* (2023a) analyzed changes in porosity within the shear box during cyclic shear, concluding that porosity near the interface is higher than in other regions. Pei *et al.* (2022) investigated energy dissipation within the soil mass, discovering that energy dissipation initially occurs in the weak force chain network and then propagates into the strong force chain network. Huang *et al.* (2019) studied interface cyclic cumulative deformation from the perspective of porosity and analyzed the correlation between final deformation under cyclic and monotonic loads. However, there is currently limited micro-analysis on factors such as particle motion, fabric anisotropy, and coordination number during horizontal cyclic shear at the granite residual soil-concrete interface.

This study aims to combine experimental methods with DEM to analyze the mechanical response of the granite residual soil-concrete interface under cyclic loading from both macroscopic and microscopic perspectives. Experimental methods will be used to study the macroscopic mechanical response of the interface, while DEM will be employed to analyze changes in microscopic parameters such as porosity, contact force chains, and fabric anisotropy, to deepen the understanding of the interaction mechanisms at the pile-soil interface under cyclic loading.

2. Experimental apparatus and methodology

2.1 Experimental equipment and materials

In direct shear tests on soil-structure interfaces, the size and boundary conditions of the shear box significantly impact the test results. However, a unified standard has not yet been established. The study utilized a large dynamic direct shear apparatus, as shown in Fig. 1, with shear box dimensions of 305 × 305 × 150 mm (top) and 405 × 305 × 150 mm (bottom), meeting the ASTM-2017 standard requirements for instrument size.

The granite residual soil used in the tests was sourced from Zengcheng District, Guangzhou City, with its particle size distribution curve shown in Fig. 2. To determine the surface roughness of the concrete, Barton *et al.* (1977)

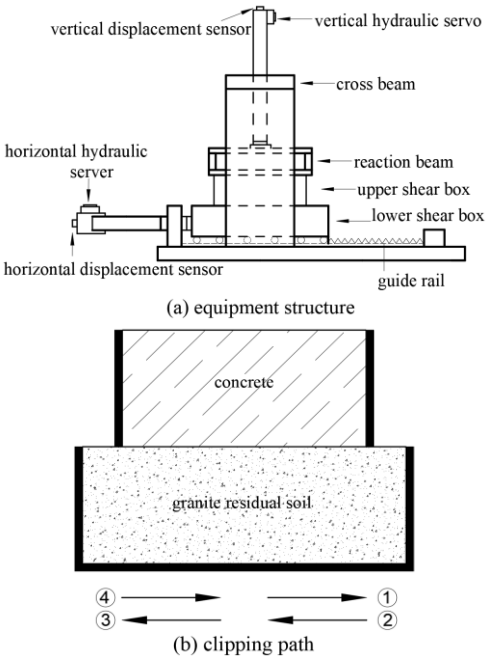

Fig. 1 Large dynamic direct shear apparatus

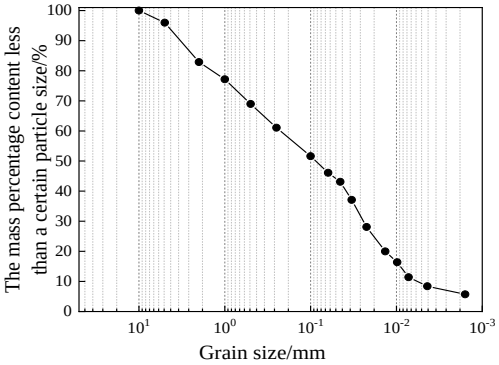

Fig. 2 Particle grading curve

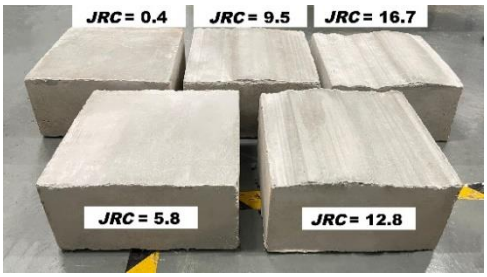

Fig. 3 Concrete test blocks with different roughness

Table 1 Test scheme

water content w/%	joint roughness coefficients	normal stress σ_n/kPa	number of classes
14, 19, 24, 29	9.5	100, 200, 300	12
14	0.4, 5.8, 12.8, 16.7	100, 200, 300	12
19, 24, 29	0.4, 5.8, 12.8, 16.7	100	12

standard structural surface roughness curve was employed, producing concrete specimens with different roughness levels (0.4, 5.8, 9.5, 12.8, 16.7). The concrete specimens were prepared according to GB/T 50081-2019 "Standards for Mechanical Properties Test Methods of Ordinary Concrete," with the specific shapes shown in Fig. 3.

2.2 Experimental procedure

The experiment aimed to study the effects of water content, roughness, and cyclic shear stress history on interface shear characteristics, with the specific test scheme detailed in Table 1. Prior to the experiment, the granite residual soil was placed into the lower shear box, filled and compacted in 5 layers to achieve a dry density of 1.4 g/cm³, and leveled. The upper shear box was then fitted with the concrete specimen. During the test, the shear load was applied in a sine wave pattern with a frequency of 0.1 Hz and a shear displacement amplitude of 3 mm. The test was stopped after 100 shear cycles, followed by a monotonic direct shear test. All test steps were conducted according to GB/T 50123-2019 "Standards for Geotechnical Test Methods."

3. Experimental results and analysis

3.1 Influence of water content on interface shear properties

Specifically, during the cyclic process, the maximum shear stresses are 82.8 kPa, 77.8 kPa, 45.2 kPa, and 37.9 kPa for water contents of 14%, 19%, 24%, and 29%, respectively. As water content increases, the maximum shear stress shows a decreasing trend, and the hysteresis loop shape transitions from vertical to horizontal. This decreasing trend in maximum shear stress with increasing water content can be explained as follows: during cyclic shearing, the energy input is primarily dissipated by the movement of soil particles. Soils with lower water content have a larger internal friction angle, leading to stronger particle interactions. Under these conditions, the rolling and rotating of soil particles must overcome greater inter-particle interlocking forces, resulting in higher shear stress levels.

Fig. 5 presents the variation of maximum interface shear stress with cyclic numbers. The variation of maximum interface shear stress is mainly concentrated in the first 20 cycles, with only slight fluctuations in subsequent cycles. At 24% and 29% water content, the maximum interface shear stress rapidly reaches its peak within the first five cycles and then gradually decreases. This attenuation phenomenon

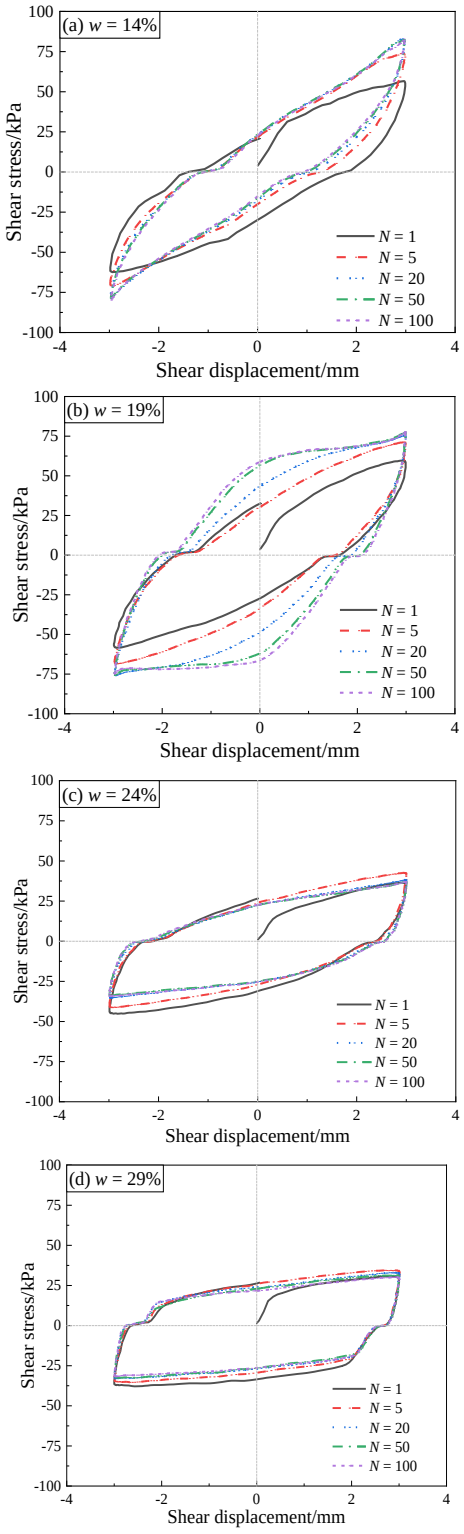

Fig. 4 Shear stress-displacement curves under different water content conditions

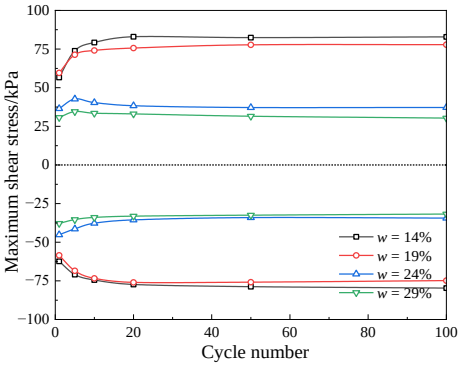

Fig. 5 Relationship between the maximum shear stress and the number of cycles

occurs because the density of the soil and the contact area between the soil and concrete do not significantly increase under cyclic loading. As cycling progresses, repeated friction at the interface smoothens the soil surface, thereby reducing shear stress.

In the same cycle, the maximum shear stress values in the forward and reverse shear directions are not completely equal. This anisotropy is partly due to the asymmetric roughness of the concrete surface in the shear direction and partly due to the rearrangement of soil particles around the interface during cyclic shearing. This rearrangement affects shear stress. In the later stages of shearing, the particle arrangement stabilizes, and the stress difference decreases.

Fig. 6 depicts the vertical displacement of soil under different water content conditions, with positive direction indicating soil compression during shearing. Since the bottom area of the shear box remains constant, the vertical displacement can indicate volume changes in the soil. Vertical displacement v can be divided into reversible vertical displacement v_{re} and irreversible vertical displacement v_{ir}. The irreversible vertical displacement v_{ir} is the maximum value of v within a single cycle, and the reversible vertical displacement v_{re} is obtained by subtracting v_{ir} from v (Feng *at al.* 2011). Comparing the starting points within a single cycle in Fig. 6 reveals that v_{ir} consistently increases, but at a decreasing rate. Consequently, the hysteresis loop remains open within a single cycle but gradually closes, with the curves tending to overlap. During the cyclic process, soil compression and dilation occur alternately, but overall compression dominates, causing subsidence and depression at the interface, with slight bulging on both sides. The higher the water content, the more pronounced the bulging.

Within a single cycle, the shearing direction reverses twice, resulting in a 180° change. During reverse shearing, the influence of forward shearing remains dominant but diminishes rapidly. Macroscopically, this manifests as increased vertical displacement and soil volume shrinkage. Microscopically, soil particles at the interface rearrange, moving from high to low potential energy. When the reverse shearing direction dominates, the particles at the interface rearrange again, rotating and rolling from low to high potential energy, leading to volume expansion. Once volume expansion peaks, another shear reversal occurs, repeating the cycle

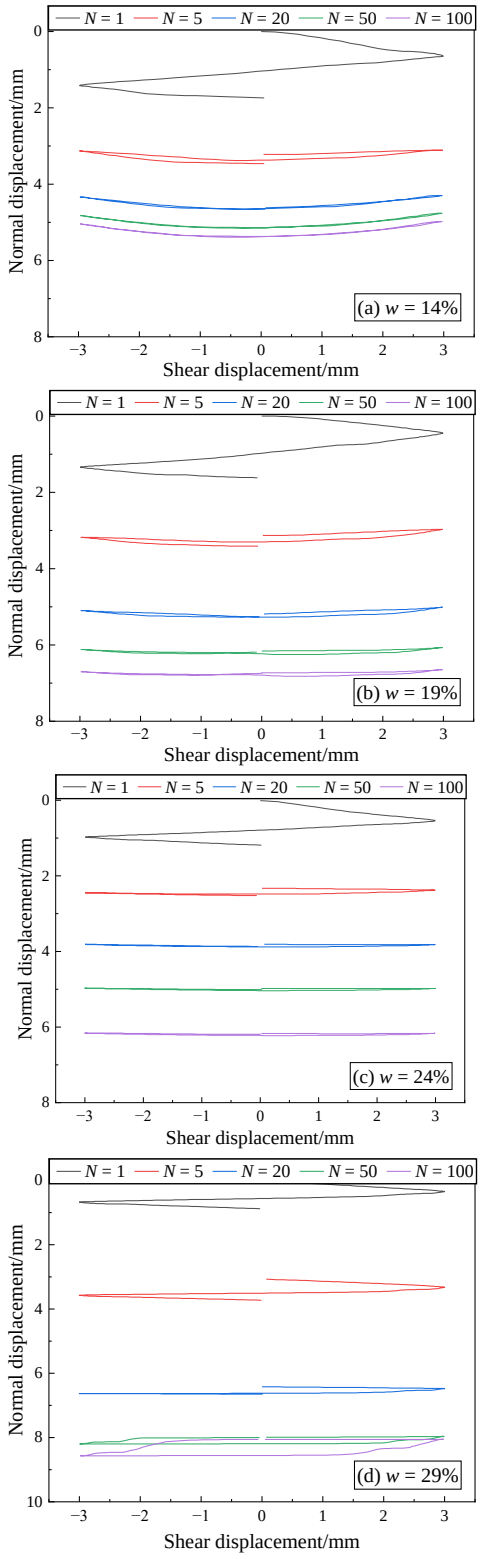

Fig. 6 Vertical displacement-shear stress curves under different water content conditions

Shear stiffness K and damping ratio D are crucial parameters in soil dynamic response, reflecting the shear deformation properties and energy dissipation of structural surfaces. The calculation methods refer to the study by YING *et al.* (2022), and the results are depicted in Fig. 7.

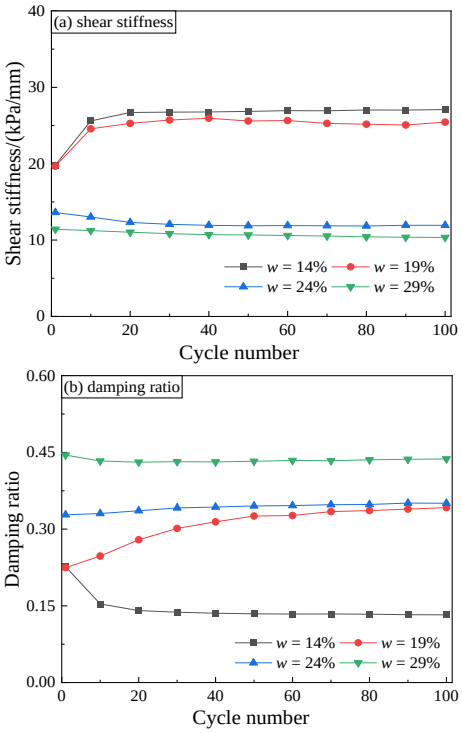

Fig. 7 The variation curves of shear stiffness and damping ratio with the number of cycles

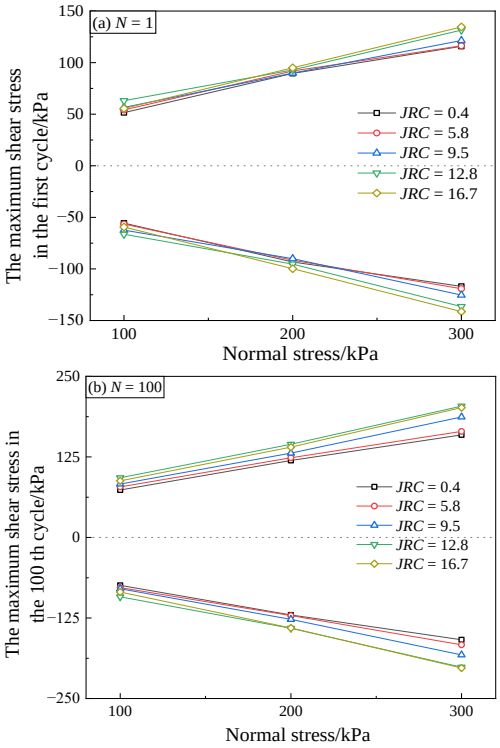

Fig. 8 The maximum shear strength of the interface under different roughness conditions

The results indicate that changes in water content significantly impact the magnitude and development pattern of shear stiffness. For low water content (14%, 19%) conditions, shear stiffness rapidly increases in the initial phase of cyclic shearing, then stabilizes; for medium to high water content (24%, 29%) conditions, shear stiffness initially weakens slowly before stabilizing. Specifically, the maximum shear stiffness of the 14% water content sample throughout the cycles is 104%, 199%, and 237% of the 19%, 24%, and 29% water content samples, respectively, demonstrating the significant impact of water content on shear stiffness.

The damping ratio under different water content conditions shows a trend opposite to that of shear stiffness; higher water content results in a larger damping ratio. This is because increased water content leads to water molecules filling the gaps between particles, forming a water film on particle surfaces, enhancing inter-particle contact. This facilitates more effective energy dissipation during cyclic shearing. Water molecules alter the soil's mechanical response, turning the soil from a granular state into a cohesive "putty" state, enhancing its elasticity and damping effect. Additionally, water molecules move within the soil pores, with stronger movement dissipating more energy. Increasing water content increases the movement of water molecules, thereby enhancing the damping effect. The damping ratio shows different patterns of change with cyclic numbers under varying water content conditions. For example, at 14% water content, the damping ratio continuously decreases with increasing cycles; at 19% water content, it increases with cycles; while at 24% and 29% water content, it remains relatively stable.

3.2 Influence of roughness on interface shear properties

Fig. 8 shows the variation curves of maximum interface shear stress with normal stress under different roughness conditions. Due to the low water content of the soil (14%), cyclic shearing exhibits a hardening phenomenon, so only the maximum shear stress for the 1st and 100th cycles is shown. The results indicate that concrete roughness significantly enhances the interface's shear resistance. For instance, at 100 kPa normal stress, increasing roughness from 0.4 to 12.8 raises the maximum forward shear stress by 22.5% and 29.4% for the 1st and 100th cycles, respectively. However, further increasing roughness reduces the maximum shear stress, indicating a critical joint roughness coefficient beyond which the mechanical properties of the interface no longer improve. This can be explained by the greater entrapment of soil in the concrete grooves with increasing roughness, reducing the effective roughness of the concrete.

Comparing the maximum shear stress of the 1st and 100th cycles reveals that the soil's shear resistance improves significantly after cyclic shearing. This is because, microscopically, soil particles continuously rearrange, altering the soil's pore structure. Macroscopically, the soil density increases, and the internal shear band develops, making force transmission more efficient and significantly improving the interface's shear strength.

The variation patterns of maximum shear stiffness and final damping ratio with roughness are shown in Fig. 9. As roughness increases, maximum shear stiffness initially increases and then decreases, indicating that selecting an

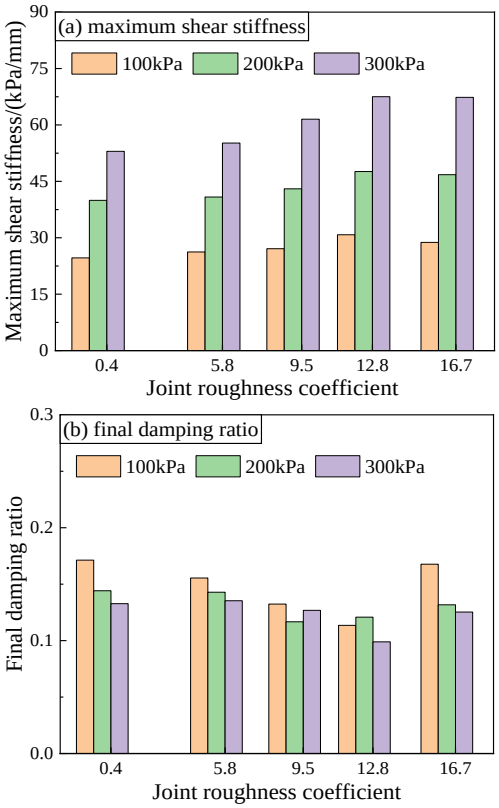

Fig. 9 The maximum shear stiffness and final damping ratio under different roughness conditions

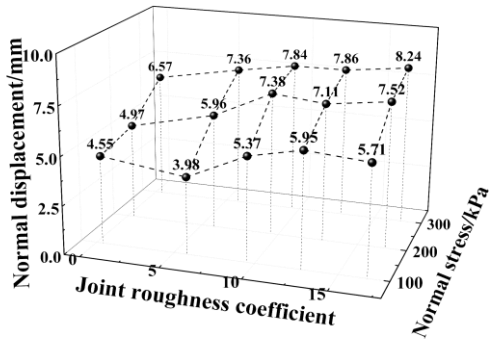

Fig. 10 Cumulative vertical displacement under different roughness conditions

appropriate structural surface roughness can enhance the mechanical properties of the interface. The increase in roughness also initially lowers and then raises the final damping ratio. Although lower roughness reduces interface shear strength, it increases the damping ratio, enhancing energy dissipation and reducing structural damage. Notably, abrupt changes occur near the critical roughness for both maximum shear stiffness and final damping ratio, providing important insights into the interaction between soil and structural surfaces. With increasing normal stress, maximum shear stiffness consistently rises, while the damping ratio continuously declines, indicating a negative correlation between maximum shear stiffness and final damping ratio at the granite residual soil-concrete interface.

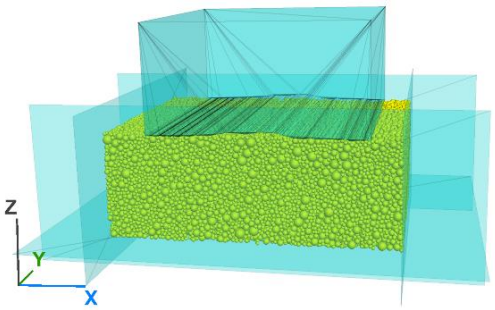

Fig. 11 Three-dimensional model of direct shear test

Table 2 Discrete element model parameters

parameter	numerical value	unit
young's modulus(Es)	8×10^7	Pa
stiffness ratio(K^*)	1	/
damping ratio(β)	0.5	/
solid friction factor(μ_p)	0.4	/
wall friction coefficient(μ_w)	0.5	/
particle density(ρ_p)	2300	kg/m³
F_0	0.2	N
D_0	0.8	mm

Fig. 10 depicts the relationship between accumulated vertical displacement, roughness, and normal stress at the granite residual soil-concrete interface. During the tests, the soil consistently exhibited compression, with accumulated vertical displacement increasing with roughness. This trend arises because higher roughness of concrete blocks causes stronger soil disturbance, making the soil on both sides of the interface more prone to bulging, leading to greater vertical displacement. As normal stress increases, the cyclic shearing effect strengthens, transforming the remolded soil from a disordered state to a more ordered one. Soil particles continuously rearrange, reducing inter-particle voids and exhibiting stronger regularity. Consequently, the accumulated vertical displacement at the interfaces of concrete blocks with five different roughnesses increases with normal stress.

4. Numerical simulation analysis of direct shear test

4.1 Model establishment and validation

The DEM software was employed to simulate indoor direct shear tests. To better simulate the cohesion between particles of granite residual soil, the "Adhesive Rolling Resistance Linear Model" contact model was used. This model adjusts the cohesion between particles through the attraction range (D_0) and the maximum cohesive force (F_0). To balance computational efficiency and size effects, the minimum particle radius was controlled at 2.5 mm, and the maximum particle radius was controlled at 7 mm. The modeling results are shown in Fig. 11, and the model parameters are listed in Table 2.

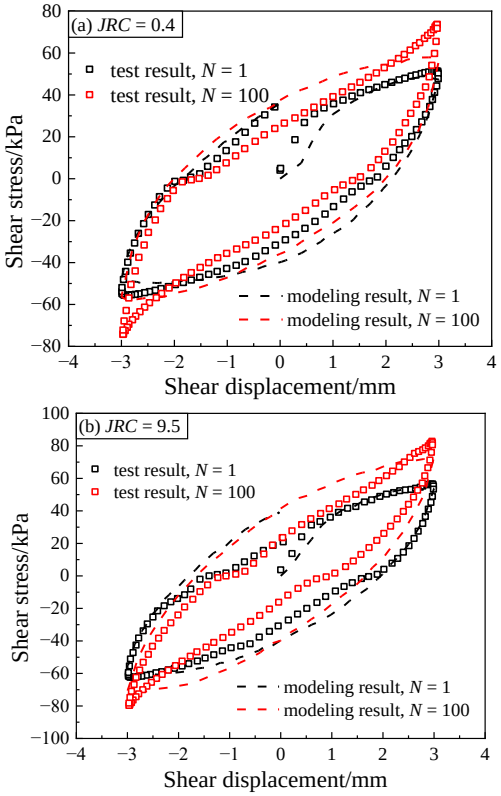

Fig. 12 Experimental and numerical simulation results

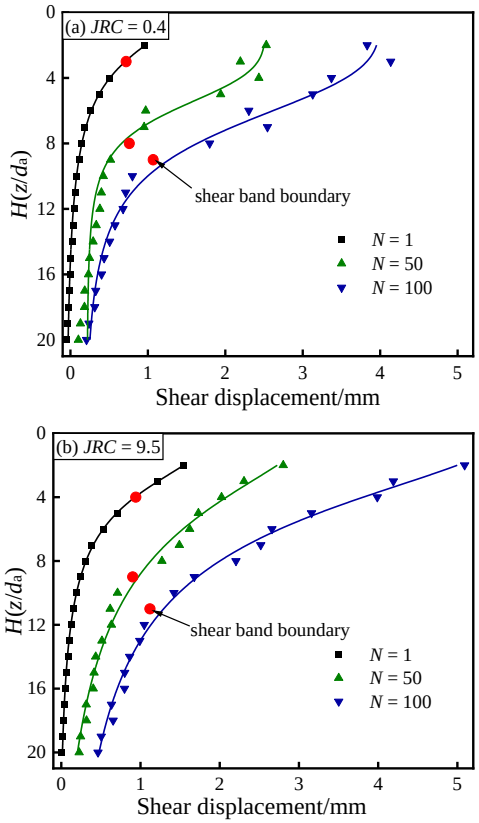

Fig. 13 Particle displacement distribution

In order to verify the accuracy of the numerical simulation results, Fig. 12 compares the shear stress-shear displacement curve curve.

4.2 Analysis of particle displacement and rotation

Fig. 13 illustrates the distribution of particle displacement (cumulative displacement) under normalized height ($H = \frac{z}{d_a}$) of the sample, where z represents the depth of the shear box, and d_a represents the average particle diameter, approximately 0.75 mm. The results indicate that particle displacement is more active near the interface. As the depth of the shear box increases, particle displacement gradually decreases, indicating that particle migration decreases with increasing distance from the interface. This phenomenon occurs because particles at the interface are influenced by friction and interlocking forces from the upper concrete, following the same motion trend as the concrete. As depth increases, this influence gradually weakens, leading to a significant demarcation point in particle displacement.

According to the study by Zhang *et al*. (2024), the shear band is a narrow region formed near the soil-concrete interface where shear deformation is concentrated. The demarcation point of this region defines the boundary of the shear band. By observing particle displacement and calculating curvature, the position of the shear band boundary was determined and marked with red dots in the Fig. 13. With increasing cyclic shear, the shear band continues to develop. Observing the depth of the shear band

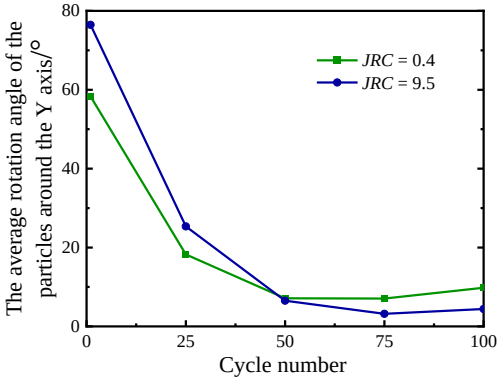

Fig. 14 The average rotation angle of the particles around the Y axis

in the 1st, 50th, and 100th cycles, it is found that the shear band gradually stops growing. This may be because the development of the shear band requires higher soil strength.

As cyclic shearing progresses, soil compaction approaches the upper limit under test conditions, thus limiting the growth of the shear band.

Comparing the two roughness conditions, it is observed that the particle displacement and shear band range are larger under rougher conditions. This is due to the geometric interlocking characteristics of concrete, which enhance the interlocking effect on the soil, thereby increasing the forces applied to the particles, leading to more extensive rearrangement.

Fig. 14 shows the average rotation angle of particles around the Y-axis within the shear band. When $N = 1$, the

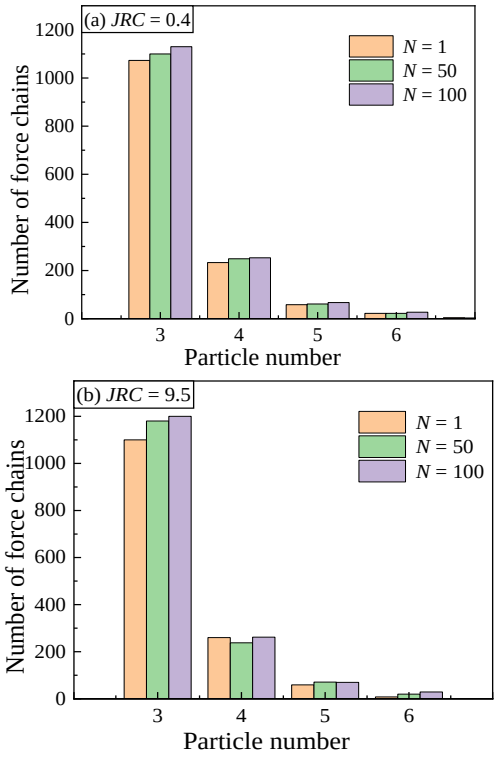

Fig. 15 The number of particles constituting the force chain

particle rotation angle is maximal and gradually decreases with the increase in cycles. This is because, in the initial stage of shearing, the sample volume significantly reduces under shearing, causing intense rolling and rotation of particles within the shear band. As cycling continues, particles move to more stable positions, establishing a more stable particle structure, which correspondingly reduces the particle rotation angle. This manifests macroscopically as a significant reduction in the sample's volume change rate.

4.3 Analysis of force chain number

To study the force transmission characteristics between particles, the concept of force chains was introduced. According to the research by Peters *et al.* (2005) and Fu *et al*. (2019), force chains should consist of three or more particles, with the absolute value of the maximum principal stress of each particle being greater than the system's average contact force. The angle between the centerline of adjacent particles in the force chain and the principal stress direction should be less than 45°.

Based on these requirements, the number of particles constituting the force chains was counted in Fig. 15. As the number of particles in the force chains increases, the number of force chains gradually decreases. This is because the more particles there are, the higher the complexity of the force chains, thereby increasing the risk of force chain breakage or failure. Additionally, with the increase in cyclic shear, the rearrangement of particles gives the sample a certain structural integrity, helping to better withstand external loads, which is reflected in the increase in the number of force chains. When roughness increased from 0.4

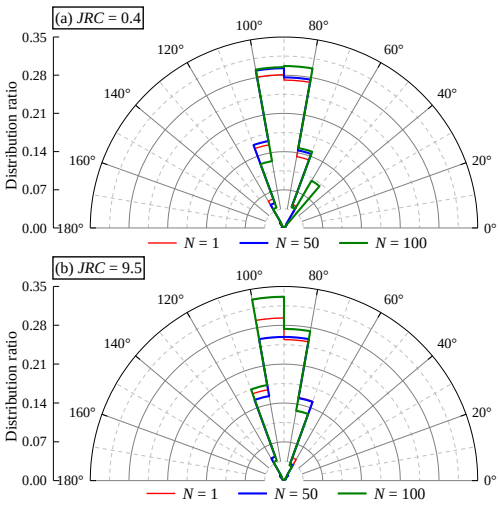

Fig. 16 Distribution of force chain angle

to 9.5, the total number of force chains increased by 3.0%, 5.4%, and 5.7% at ($N=1$), ($N=50$), and ($N=100$), respectively. This indicates that the roughness of the concrete surface affects force transmission and the formation of force chains, thereby influencing the macroscopic shear strength of the interface.

4.4 Analysis of force chain angle

The angle of a force chain is defined as the angle between the vector formed by the centroids of the first and last particles and the positive direction of the z-axis. Fig. 16 shows the distribution of force chain angles, with most force chain angles concentrated between 70° and 110°, indicating that force chains are mainly distributed horizontally. This may be because shear occurs at the interface, resulting in higher shear stress near the interface, creating a "stress concentration" phenomenon. Meanwhile, normal stress is applied relatively evenly on the sample, leading to fewer force chains in the normal direction. With the increase in cycles, the distribution difference of force chain angles becomes more significant under a roughness of 9.5. Higher roughness levels cause more intense motion during interface shearing, directly affecting the structure and stability of the force chains, leading to greater fluctuations in force chain angle distribution

4.5 Analysis of force chain structure index

Liu *et al.* (2023b) proposed the Force Chain Structure Index (MFCSI) to measure the length and bearing capacity of force chains, calculated by Eq. (1). The smaller the MFCSI value, the lower the bearing capacity and the shorter the length of the force chains. As shown in Fig. 17, under both roughness conditions, the cumulative curve development of the structural index is similar, with MFCSI mainly distributed below 100, indicating that shorter and weaker force chains are easily formed in the sample.

$$\mathrm{MFCSI}_i = \sum_{k=1}^{S} f_k d_k \tag{1}$$

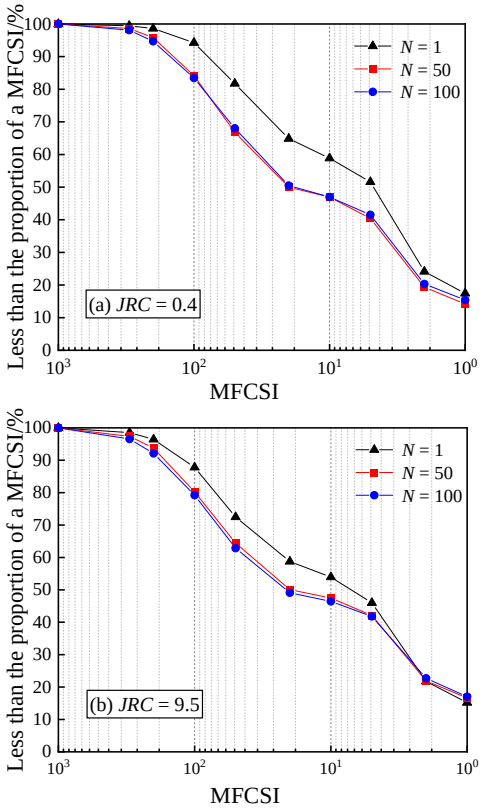

Fig. 17 Force chain structure index cumulative curve

In the formula, S represents the total number of contacts in the i th force chain ; f_k denotes the magnitude of the k th contact force in the i th force chain ; d_k is the sum of the radii of two particles near the contact point.

4.6 Analysis of fabric anisotropy

The macroscopic strength characteristics exhibited by the sample during shearing are closely related to the evolution of the particle microstructure. Rothenburg and Bathurst (1989) proposed that the anisotropy of normal contact force and tangential contact force between particles during direct shear tests can be approximated by a Fourier function, mathematically expressed as follows

$$f_n(\theta) = f_0\left[1 + a_n \cos 2(\theta - \theta_n)\right] \tag{2}$$

$$f_t(\theta) = -f_0 a_t \sin 2(\theta - \theta_t) \tag{3}$$

In the formula, a_n and a_t represent the anisotropy coefficient of normal contact force and tangential contact force respectively, θ_n and θ_t represent the main direction of anisotropy of normal contact force and tangential contact force respectively, and f_0 represents the average contact force.

Figs. 18 and 19 show the normalized distribution of normal and tangential contact forces projected onto the (xoz) plane. In the initial state, the particles are mainly influenced by gravity and normal contact forces, so the principal direction of anisotropy is close to 90°, with normal and tangential contact forces showing symmetrical distribution characteristics along the vertical direction. When shearing begins, the principal direction of anisotropy rotates by about 35° along the shearing direction. During the shearing process, the rotation angle and average contact force of the sample with a roughness of 9.5 are always greater than those of the sample with a roughness of 0.4. This indicates that the higher the roughness, the more intense the disturbance to the pa rticles during shearing, the greater the rotation of the principal direction along the shearing direction, and the greater the contact force generated between particles.

5. Conclusions

Through large-scale indoor direct shear tests, the influence of moisture content and roughness on the macroscopic shear characteristics of the residual soil-concrete interface was studied. Numerical simulations were used to analyze the micromechanical behavior during shearing, leading to the following conclusions:

- The relationship between shear stress and displacement at the residual soil-concrete interface is related to the soil moisture content. At low moisture content (14%, 19%), a trend of cyclic shear hardening is observed, while at high moisture content (24%, 29%), a trend of cyclic shear softening is observed.
- As roughness increases, the maximum shear stiffness of the interface continuously grows. However, after reaching a critical roughness value, it no longer increases, and the final damping ratio of the interface exhibits an opposite trend.
- The thickness of the shear band increases with cyclic shear and is proportional to the roughness of the concrete surface.
- The principal direction of anisotropy for normal and tangential contact forces rotates by about 35° along the shearing direction. With increasing concrete surface roughness, the principal direction's rotation becomes more pronounced.

Acknowledgments

This study was supported by the National Natural Science Foundation of China (Grant No.s 52378355 and 52078285). We gratefully acknowledge the financial support.

References

Barton, N.R. and Choubey, V. (1977), “The shear strength of rock joints in theory and practice”, *Rock Mech.*, **10**, 1-53. https://doi.org/10.1007/BF01261801.

Bathurst, R.J. (1989), “Analytical study of induced anisotropy in idealized granular materials”, *Géotechnique*, **39**(4), 601-614. https://doi.org/10.1680/geot.1989.39.4.601.

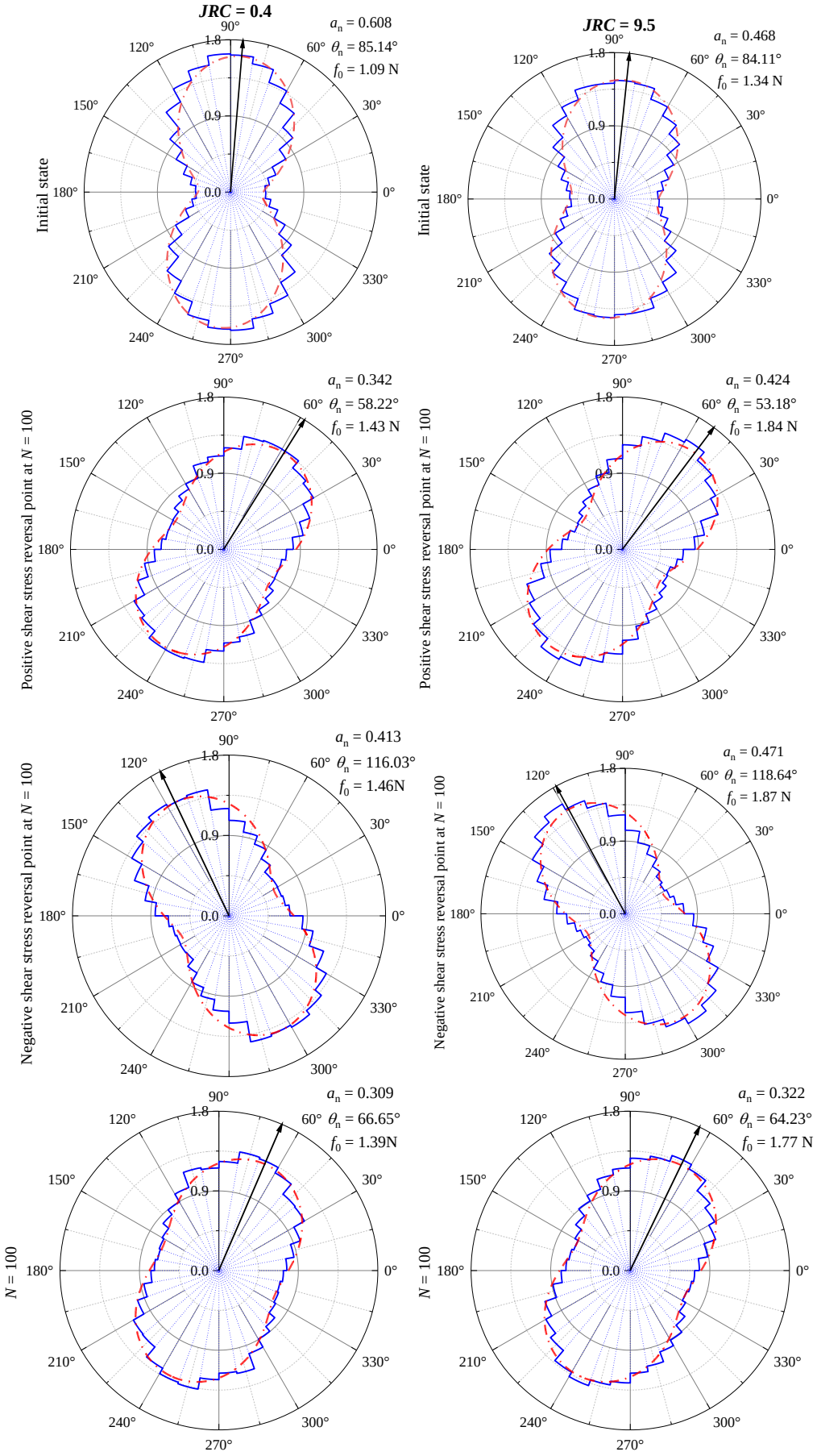

Fig. 18 Normal contact force normalized distribution

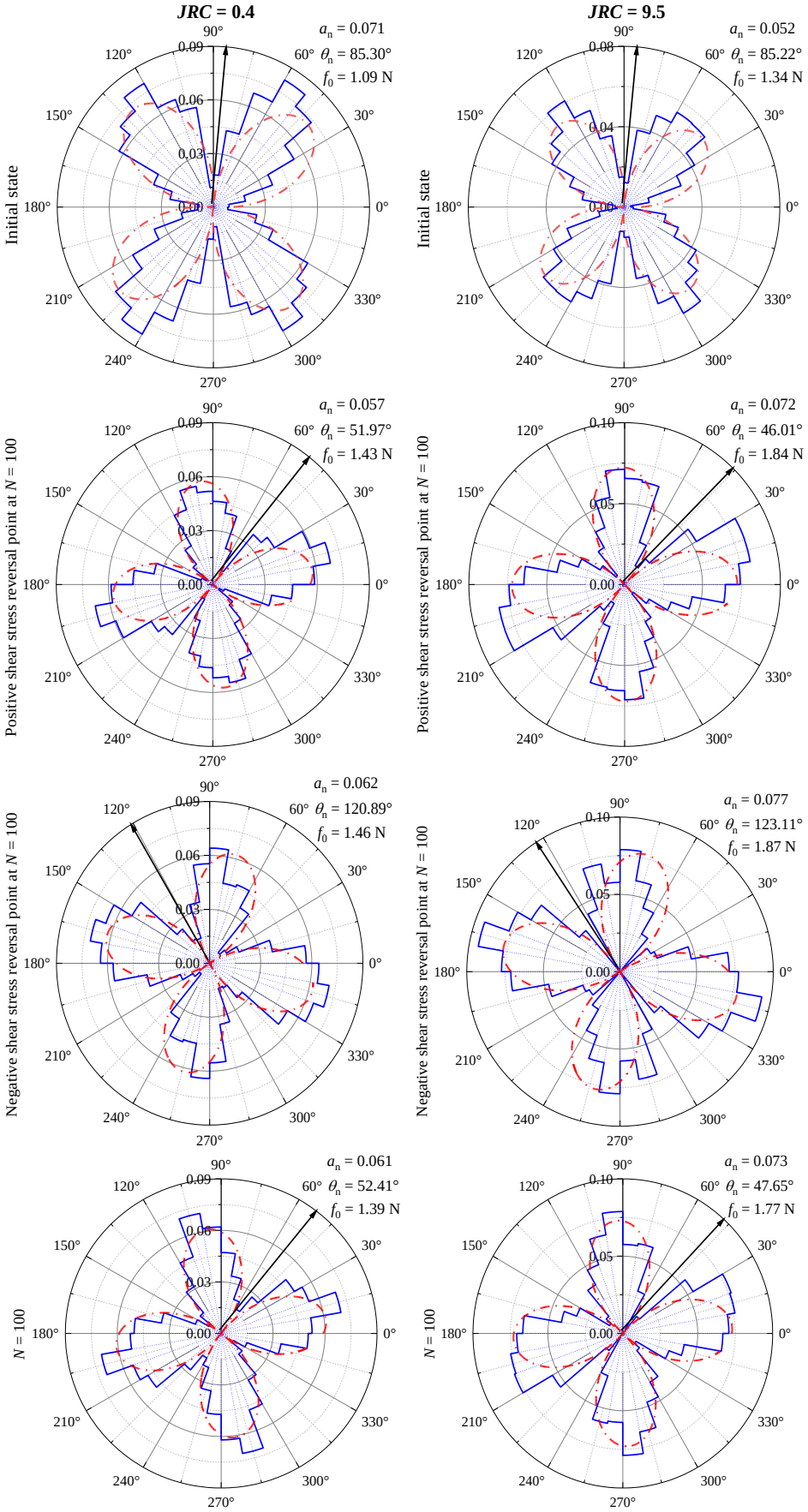

Fig. 19 Tangential contact force normalized distribution

Chen, X.B., Zhang, J.S., Xiao, Y.J. and Li, J. (2015), "Effect of roughness on shear behavior of red clay - concrete interface in large-scale direct shear tests", *Can. Geotech. J.*, **52**(8), 1122-1135. https://doi.org/10.1139/cgj-2014-0399.

Chen, C., Yang, Q., Leng, W.M., Dong, J.L., Xu, F., Wei, L.M. and Ruan, B. (2022), "Experimental investigation of the mechanical properties of the sand-concrete pile interface considering roughness and relative density", *Materials*, **15**(13), 4480. https://doi.org/10.3390/ma15134480.

Chen, W.B., Zhou, W.H. and Yin, Z.Y. (2023), "Recent development on macro-micro mechanism of soil-structure interface shearing through DEM", *Arch. Comput. Method. Eng.*, **30**(3), 1843-1862. https://doi.org/10.1007/s11831-022-09854-0.

Dou, H.Q., Xie, S.H., Chen, F., Wang, H., Chen, F.Q. and Jian, W.B. (2023), "Study on shear characteristics and a mechanics model of granite residual soil-rock interface", *Bull. Eng. Geol. Environ.*, **82**(6), 212. https://doi.org/10.1007/s10064-023-03220-5.

Fang, H.L. and Wang, W.J. (2020), "A three-dimensional multishear bounding surface model of granular soil-structure interfaces under monotonic and cyclic loading", *J. Eng. Mech.*, **146**(7), 04020068. https://doi.org/10.1061/(ASCE)EM.1943-7889.0001796.

Feng, D.K., Hou, W.J. and Zhang, J.M. (2011), "Test investigations on 3D stress-controlled cyclic behavior of gravel-structure interface", *Chinese J. Rock Mech. Eng.*, **30**(12), 2574-2582. http://doi.org/CNKI:SUN:YSLX.0.2011-12-024.

Feng, D.K. and Zhang, J.M. (2022), "Influences of shear stress amplitude on tangential deformation behavior of a gravel-structure interface", *Chinese J. Geotech. Eng.*, **44**(11), 1959-1967. http://dx.doi.org/10.11779/CJGE202211001.

Fu, L.L., Zhou, S.H., Guo, P.J., Wang, S. and Luo, Z. (2019), "Induced force chain anisotropy of cohesionless granular materials during biaxial compression", *Granular Matter.*, **21**(3), 52. https://doi.org/10.1007/s10035-019-0899-1.

Huang, M.S., Chen, Y.W. and Gu, X.Q. (2019), "Discrete element modeling of soil-structure interface behavior under cyclic loading", *Comput. Geotech.*, **107**, 14-24. https://doi.org/10.1016/j.compgeo.2018.11.022.

Li, L.C., Zheng, M.Y., Liu, X., Wu, W.B., Liu, H., El Naggar, M. H. and Jiang, G.S. (2022a), "Numerical analysis of the cyclic loading behavior of monopile and hybrid pile foundation", *Comput. Geotech.*, **144**, 104635. https://doi.org/10.1016/j.compgeo.2022.104635.

Li, S.J., Tong, Y.G., Wang, J., Ying, M.J. and Liu, F.Y. (2022b), "Cyclic shear properties of gravel-geogrid interface under bidirectional cyclic loading", *Rock Soil Mech.*, **43**(2), 291-298. https://link.cnki.net/doi/10.16285/j.rsm.2021.0357.

Li, X., Liu, Y.Y., Qian, G.P., Liu, X.Q., Wang, H. and Yin, G.Q. (2023), "Numerical investigation into particle crushing effects on the shear behavior of gravel", *Geomech. Eng.*, **35**(2), 209-219. https://doi.org/10.12989/gae.2023.35.2.209.

Liu, S.A., Liao, C.C., Chen, J.J., Ye, G.L. and Xia, X.H. (2021a), "Strength properties of saturated sand-structure interface by triaxial test method", *J. Shanghai Jiaotong Univ.*, **55**(11), 1371-1379. https://link.cnki.net/doi/10.16183/j.cnki.jsjtu.2020.299.

Liu, F.Y., Ying, M.J., Yuan, G.H., Wang, J., Gao, Z.Y. and Ni, J.F. (2021b), "Particle shape effects on the cyclic shear behaviour of the soil-geogrid interface", *Geotext. Geomembranes*, **49**(4), 991-1003. https://doi.org/10.1016/j.geotexmem.2021.01.008.

Liu, F.Y., Zhu, C. and Wang, J. (2021c), "Influences of shear rate and loading frequency on shear behavior of geogrid-soil interfaces", *Chinese J. Geotech. Eng.*, **43**(5), 832-840. http://dx.doi.org/10.11779/CJGE202105006.

Liu, F.Y., Fu, J., Lu, Y. and Ying, M.J. (2023a), "Macro and micro analyses of static and dynamic shear characteristics of geogrid and rubber-sand mixture interface", *Transport. Geotech.*, **43**, 101119. https://doi.org/10.1016/j.trgeo.2023.101119.

Liu, G.Q., Huang, T., Lyu, L., Liu, Z.J. and Ma, C.Z. (2023b), "Effective load transfer capacity analysis for asphalt mixture skeleton based on main force chain characteristics and discrete element method", *J. Mater. Civil Eng.*, **35**(9), 04023303. https://doi.org/10.1061/JMCEE7.MTENG-15997.

Ma, Y.M., Guo, J.K., Wang, R., Zhang, Q.Y., Zhang, Q.X., Li, J. and Zuo, S. (2023), "Study on cyclic shear properties of siliceous sand-steel interface under different normal loading conditions", *Buildings*, **13**(9), 2241. https://doi.org/10.3390/buildings13092241.

Maghsoodi, S., Cuisinier, O. and Masrouri, F. (2020), "Effect of temperature on the cyclic behavior of clay-structure interface", *J. Geotech. Geoenviron. Eng.*, **146**(10), 04020103. https://doi.org/10.1061/(ASCE)GT.1943-5606.0002360.

Mamen, B. and Hammoud, F. (2021), "Microstructural observations of shear zones at cohesive soil-steel interfaces under large shear displacements", *Geomech. Eng.*, **25**(4), 275-282. https://doi.org/10.12989/gae.2021.25.4.275.

Mirzaalimohammadi, A., Ghazavi, M., Roustaei, M. and Lajevardi, S.H. (2019), "Pullout response of strengthened geosynthetic interacting with fine sand", *Geotext. Geomembranes*, **47**(4), 530-541. https://doi.org/10.1016/j.geotexmem.2019.02.006.

Pei, T. and Qiu, T. (2022), "DEM investigation of energy dissipation at particle contacts in granular soil under cyclic torsional shear", *Int. J. Geomech.*, **22**(4), 04022016. https://doi.org/10.1061/(ASCE)GM.1943-5622.0002304.

Peters, J.F., Muthuswamy, M., Wibowo, J. and Tordesillas, A. (2005), "Characterization of force chains in granular material", *Phys. Review E*, **72**(4), 041307. https://doi.org/10.1103/PhysRevE.72.041307.

Qi, T., Zhao, C., Liu, F.Y. and He, J.H. (2023), "Study on cyclic shearing characteristics of sulfated soil-concrete interface", *Chinese J. Rock Mech. Eng.*, **42**(2), 4280-4288. https://link.cnki.net/doi/10.13722/j.cnki.jrme.2022.1055.

Wang, X., Cheng, H., Yan, P., Zhang, J.S. and Ding, Y. (2021), "The influence of roughness on cyclic and post-cyclic shear behavior of red clay-concrete interface subjected to up to 1000 cycles", *Constr. Build. Mater.*, **273**, 121718. https://doi.org/10.1016/j.conbuildmat.2020.121718.

Yang, J.C., Xia, Y.Y., Chen, W.D., Zhang, L. and Li, L.H. (2023), "Shear behavior of silty clay-concrete interface based on large-scale direct shear test", *Int. J.of Geomech.*, **23**(7), 04023084. https://doi.org/10.1061/IJGNAI.GMENG-828.

Ying, M.J., Wang, J., Liu, F.Y., Li, J.T. and Chen, S.Q. (2022), "Analysis of cyclic shear characteristics of reinforced soil interfaces under cyclic loading and unloading", *Geotext. Geomembranes*, **50**(1), 99-115. https://doi.org/10.1016/j.geotexmem.2021.09.004.

Zhang, S.X., Liu, F.Y., Zeng, W.X. and Ying, M.J. (2024), "Analyzing cyclic shear behavior at the sand-rough concrete interface: An experimental and DEM study across varying displacement amplitudes", *Int. J. Numer. Anal. Method. Geomech.*, **48**(7), 1907-1928. https://doi.org/10.1002/nag.3713.

Zhou, W.H., Jing, X.Y., Yin, Z.Y. and Geng, X.Y. (2019), "Effects of particle sphericity and initial fabric on the shearing behavior of soil-rough structural interface", *Acta Geotechnica*, **14**(6), 1699-1716. https://doi.org/10.1007/s11440-019-00781-2.